http://dx.doi.org/10.5012/bkcs.2014.35.4.1077

Synthesis and Optical Characteristics of PAM/HgS Nanocomposites

Dezhi Qin,[*] Guangrui Yang,[†] Li Zhang, Xian Du, and Yabo Wang

College of Chemistry and Chemical Engineering, Pingdingshan University, Pingdingshan 467000, P.R. China
[*]E-mail: dezhiqin@163.com
[†]Institute of Environmental and Municipal Engineering, North China University of Water Conservancy and Electric Power, Zhengzhou 450011, P.R. China
Received October 21, 2013, Accepted November 1, 2013

Polyacrylamide (PAM) -HgS nanocomposites were successfully prepared in polyacrylamide (PAM) matrix. From TEM and XRD characterizations, the synthesized HgS nanocrystals were chain-like spherical in shape with a diameter of about 40-60 nm and high crystalline quality. The quantum-confined effect of HgS nanocrystals was confirmed by UV-vis diffuse reflection spectra. The optical properties of products were investigated by using photoluminescence (PL) spectra, which showed that HgS nanocrystals exhibited good optical properties with maximum emission peak at about 640 and 650 nm at different reaction temperatures. The interaction of HgS nanocrystals with PAM was studied through FT-IR spectroscopy and TG analysis, which suggested that Hg^{2+} could interact with functional groups of PAM. The experimental results indicated that PAM not only induced nucleation, but also inhibited further growth of HgS crystals and play an important role in the formation of PAM/HgS nanocomposites. In addition, the possible mechanism of HgS nanoparticles growth in PAM solution was also discussed.

Key Words : HgS, Nanocomposites, Polymer, Optical properties

Introduction

The study on inorganic-organic nanocomposites has attracted much attention due to their unusual optical, electrical, magnetic and mechanical properties.[1-4] In the past few years, significant progress has been made on these materials, and various approaches have been reported to synthesize inorganic-organic hybrid nanomaterials, such as micelle and microemulsion templates,[5] sol-gel process,[6] sonochemistry, microwave radiation,[7] biomimetic method,[8] Langmuir-Blodgett (LB) method,[9] hydrothermal,[2] solvothermal[10] and others. As the representative of these materials, polymer/metal chalcogenides nanocomposites have been extensively investigated because of their great potential in optoelectronic applications in the fields of light-emitting diodes (LEDs), solar cells, sensors and optical recording materials. Many polymers have been adapted as matrix to prepare metal chalcogenides nanocrystals, which bind tightly to the nanoparticles surface and in the reaction act as both solvents and capping agents. The polymers can provide functional groups and steric hindrance to control the morphology of nanocrystals, and surface passivation by polymers helps to achieve size selectivity, prevent agglomeration and control photoluminescence. On the other hand, the interaction of polymers and chalcogenides on the nanoscale level can produce some novel properties, which are not present for either of the materials alone. For example, Qian *et al.* have reported on the synthesis of polyvinylpyrrolidone (PVP) films containing silver sulfide nanoparticles.[1] Zhu *et al.* successfully prepared the HgS nanotubes by PVP-assisted photochemical route.[11] Soltani *et al.* prepared well-dispersed CdS nanoparticles in PVP solution through microwave method.[12] In these cases, the interaction of polymers with nanocrystals is necessary to provide chemical passivation, and also to improve the surface state which has significant influence on optical and electrical properties of chalcogenides nanocrystals.

Mercury is a toxic metal that is widespread in the environment and harmful to human and mammalian. The different chemical forms (organic and inorganic) of mercurial compounds exhibit different degrees of toxicity with effects including hearing loss, vision disturbance, motor deficits, and retarded or abnormal walking ability. Interestingly, in China, the ancients believed cinnabar mercury sulfide (HgS) can be made into invigorating pills called "Zhuasha" through heating, which can be as traditional Chinese medicine for soothing the nerves of human.[13] Mercury sulfide, as well as other chalcogenides, has good optical and electrical properties and is widely used in many fields including ultrasonic transducers, electrostatic image materials, photoelectric conversion devices and infrared sensors.[14-17] Because of the difficulty in synthesis and toxicity of mercury, there are very small reports on synthesis and characteristics of HgS nanocrystals.[18,19] Polymers such as polyvinylpyrrolidone (PVP), polyacrylonitrile (PAN), polyacrylamide (PAM) have been extensively utilized for the fabrication of hybridization of semiconductor nanocrystals based on polymer matrix.[1,2,11,12,20-24] The present study is aimed to synthesize polyacrylamide (PAM) -HgS nanocomposites at low temperature and ambient pressure and investigate their optical properties. The influence of temperature on the morphology and optical properties was systematically studied. The X-ray diffraction (XRD) and transmission electron microscopy (TEM) have

been carried out to study the structure and morphology of PAM/HgS nanocomposites. The optical properties of products were characterized by ultraviolet-visible (UV-vis) and photolu- minescence (PL) spectra.

Experimental

Materials. Acrylamide (AM) and azodiisobutyronitrile (AIBN) used in this study were purchased from Sinopharm Chemical Regent Co., Ltd., P.R. China. Mercury acetate [$Hg(Ac)_2$] was purchased from Taixing Chemical Co. Ltd., P. R. China. All reagents were of analytical grade without further purification. Water used in all synthesis procedures was high purity grade with a conductivity of 18.2 $M\Omega \cdot cm^{-1}$.

Synthesis of PAM/HgS Nanocomposites. In a typical preparation process, 0.96 g $Hg(Ac)_2$ and 3 g acrylamide were dissolved in 100 mL ethylene glycol under vigorous magnetic stirring to form a homogeneous solution, within N_2 atmosphere, 0.1 g AIBN was added to above solution at 60 ºC for 30 min. The H_2S gas was introduced into reaction system to form HgS nanocrystals. The color of mixed solution gradually changed from brown to dark black. Finally, the obtained black precipitates were filtered off, washed with distilled water and ethanol, and dried in a vacuum at 50 ºC for 8 h.

Characterization of PAM/HgS Nanocomposites. Powder X-ray diffraction (XRD) was carried out on a Bruker D8 Advance X-ray diffractometer using Cu Kα radiation with the scanning 2-theat angle ranging from 20 to 70 degree. The morphology of PAM/HgS nanocomposites was determined using JEOL JEL-2010 transmission electron microscopy (TEM). Fourier transform infrared (FT-IR) spectra were taken on Bruker Tensor-37 spectrophotometer in the wave number range of 4000 to 400 cm^{-1}. The ultraviolet-visible (UV-vis) diffuse reflection spectra of HgS nanocrystals have been measured at room temperature using Shimadzu UV-2550 spectrophotometer. The photoluminescence (PL) spectra were performed on a Hitachi F-7000 FL spectrophotometer with a 450 W xenon lamp as excitation source. All the optical measurements were performed at room temperature under ambient conditions.

Results and Discussion

The formation of HgS nanocrystals in PAM matrix can be confirmed by powder X-ray diffraction (XRD) study. Figure 1a shows the XRD pattern of PAM/HgS nanocomposites. The XRD pattern of HgS synthesized in PAM matrix exhibit prominent broad peaks at 2θ values of 26.8°, 30.7°, 43.6°, 52.3° and 54.1°, which could be indexed to the {111}, {200}, {220}, {311} and {222} direction of the cubic zinc blende phase (β-HgS, space group F43m) in close agreement with JCPDS (No. 06-0621) data. A broad non-crystalline peak (20-30º) is assigned to PAM polymer phase. No other characteristic peaks corresponding to impurities are found, showing the high purity of PAM/HgS nanocomposites. The presence of the broad XRD peaks indicates that the products

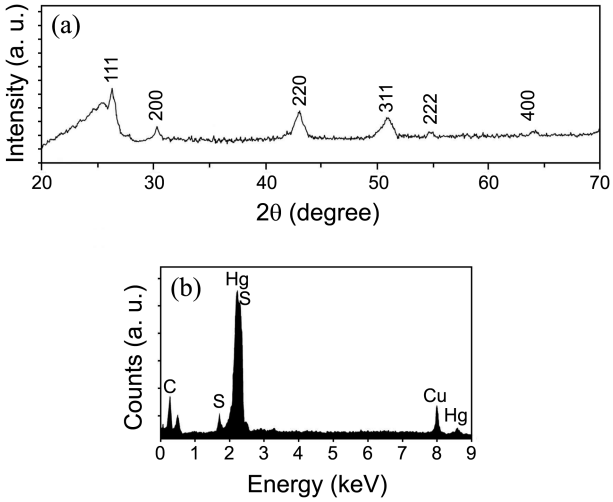

Figure 1. (a) XRD pattern and (b) EDX spectrum of PAM/HgS nanocomposites.

are composed of crystalline HgS and poorly crystalline or amorphous PAM. The crystalline size can be calculated with Scherrer's equation below[25]

$$D = \frac{k\lambda}{\beta \cos\theta}$$

where D is the mean crystalline size, k is the constant (shape factor, appromately 1), β is the X-ray wavelength (1.54056 Å for Cu-Kα), β is the full width at half maxium (FWHM) of the diffraction peak and θ is the Bragg diffraction angle. The grain size of HgS nanocrystals as calculated by using equation is 8.6 nm. The energy dispersive X-ray (EDX) analysis of PAM/HgS nanocomposites is shown in Figure 1b. In the EDX spectrum, the peaks of Hg and S are pronounced and no other peaks are found except for those of C and Cu originating from the Cu micro-grid with amorphous carbon used to support the HgS nanocrystal. The molar ratio of Hg and S is 1.13:1, which is nearly in agreement with the stoichiometric molar ratio of mercury (II) sulfide.

The shape and size of nanocrystals are significantly affected by reaction temperature. Transmission electron microscope (TEM) images of as-obtained PAM/HgS nanocomposite at different temperature are shown in Figure 2. It is becoming clear that obvious aggregation is associated with lower reaction temperature (40 ºC, Figure 2(a)). We considered that the acrylamide dimmer can not be polymerized completely at lower temperature, which result in lower concentration of PAM in solution. As a result, PAM can not control the nucleation and growth of HgS crystals effectively as matrix. Figure 2(b) shows the typical TEM image of PAM/HgS nanocomposites synthesized at 60 °C. From the figure, the large quantity HgS nanoparticles are achieved with average diameter 41.47 ± 0.21 nm, and the size distribution is given in Figure 2(f), which is approximately fit the Gaussian curve. Most of the particles are approximately spherical in shape with good uniformity; a very small number of particles are relatively of bigger size due to agglomeration of smaller particles during aging. It can be clearly observed

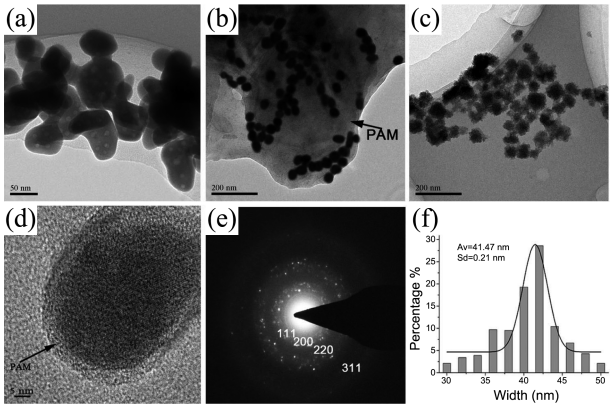

Figure 2. Typical TEM images of PAM/HgS nanocomposites synthesized at different temperature ((a) 40 ºC, (b) 60 ºC, (c) 75 ºC), (d) HRTEM image of HgS nanocrystals synthesized at 60 ºC, (e) SAED pattern of HgS nanocrystals, (f) histogram of HgS nanoparticle-size distribution synthesized at 60 ºC.

that the particles are in close contact with each other to form chains. It seems that PAM matrix has great effects on the dispersion of HgS nanoparticles, which tend to array according to the polymer matrix. In addition, HgS nanoparticles are coated by amorphous PAM thin film, as indicated by the arrow in Figure 2(b), which means the as-obtained products are inorganic-polymer composites. For reaction above 75 °C, the reaction rate increased sharply with temperature. The diameter of HgS nanoparticle is increased up to 50-60 nm (Figure 2(c)) and the products at 75 °C are predominantly a mixture of aggregated structures with a few spherical and irregular nanoparticles. Because of the higher temperature, the nucleation of HgS continued during the HgS crystal growth, thereby resulting in the wider size distribution of HgS particle. This result illustrates how the nanoparticle size can be effectively controlled by setting the reaction temperature. With the increase of temperature, the morphology and size of HgS particles could not be effectively handled. We speculated that the decomposition of AIBN at high temperature (above 70 ºC) resulted in irregular morphology and agglomeration of HgS particles. In our synthesis, the reaction temperature was the key parameter to control the size and morpholopy of HgS nanocrystals, and the optimal reaction temperature is 60 ºC. The average size of HgS nanoparticle observed from TEM is about 40 nm, which is much larger than the grain size (8.6 nm) calculated from Scherrer's equation. It could be interpreted that the obtained products are polycrystalline particles, which is also confirmed by SAED characterization (see below).

Because HgS crystals are highly sensitive to the electron beam, we have not obtained clearly detailed HRTEM image in Figure 2d. However, from HRTEM image, the edge of the nanoparticle looks fuzzy and no lattice planes is observed in this area, which indicate that most of the surface of HgS nanoparticle is covered with PAM and further confirmed amorphous nature of PAM. Accordingly, the nanocrystal size calculated from XRD is smaller than those observations from TEM and HRTEM images. The SAED pattern (Figure 2(e)) of HgS nanocrystals consists of discrete spots and fuzzy rings, which suggest that the products are composed of crystals and amorphous materials.

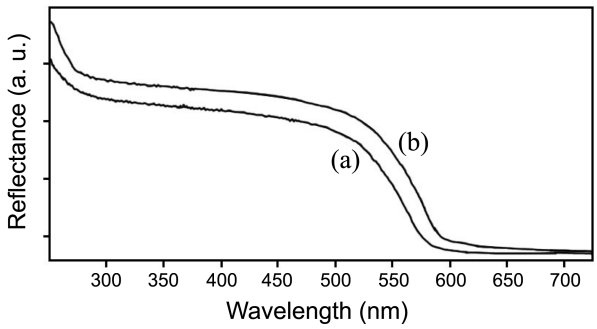

Figure 3. UV-vis reflectance spectra of PAM/HgS nanocomposites synthesized at (a) 60 ºC, (b) 75 ºC.

The ultraviolet-visible (UV-vis) diffuse reflection spectra of HgS nanocrystals synthesized in PAM matrix at 60 and 75 ºC are shown in Figure 3. Although, both curves do not show any marked sharp peaks which are replaced by long tailing. The tailing of the absorption features of HgS nanocrystals may be due to different size distribution in PAM matrix. Comparing with the reflectance spectra recorded at different reaction temperature, there is an obviously red-shift after raising temperature suggesting that the size of the nanoparticle increases. The UV-vis spectra were used to calculate the band gap from

$$\alpha(v) = A(hv/2 - E_g)^{m/2}$$

where α is the absorption coefficient and E_g is the band gap. For a direct transition m = 1, plots of $(\alpha E_{phot})^2$ *vs.* E_{phot} were constructed and the value of E_{phot} extrapolated to $\alpha = 0$ gives the band gap, E_g (Figure 4). It shows that as the reaction temperature is decreased from 75 to 60 ºC, band gap is found to be increased from 2.28 to 2.39 eV. The imposed spatial restriction on decreasing particle size increases the energy of separation between the ground and the excited electronic states as expected from the particle in an infinite potential

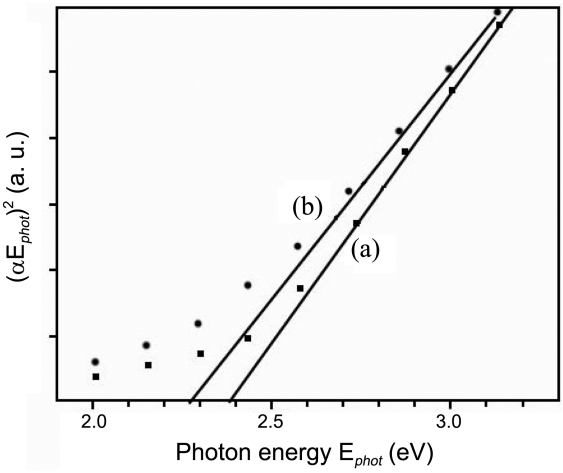

Figure 4. Plots of $(\alpha E_{phot})^2$ *vs.* E_{phot} for direct transitions of HgS nanocrystals synthesized at a: 60 ºC, b: 75 ºC.

well model which results in the blue shift of the absorption with enhancement of optical band gap of the material compared to the bulk phase (quantum confinement effect).[26] It is possible to tune the band gap of nanocrystals by controlling the particle size and to, in principle, achieve targeted optical properties.

The photoluminescence (PL) spectra of HgS nanocrystals synthesized at 60 and 75 ºC excited by the 385 nm wavelength (λ_{ex}) are shown in Figure 5. The maximum peaks of PL emissions are detected at wavelength of 642 and 653 nm, while the corresponding reaction temperatures are 60 and 75 ºC, respectively. Since the electronic energy levels of semiconductor nanocrystals are radically affected by their size, the PL peak red-shifted from 642nm to 653nm, indicating the growth of HgS nanocrystals with a raise of temperature. TEM and UV-vis characterizations indicate there is descending trend in particle size with the decrease of temperature, which is in good agreement with PL results. Ordinarily, photoluminescence emission can be obtained from semiconductor nanocrystals: a sharp excitonic emission resulting from band-to-band recombination and another broad emission at a longer wavelength due to surface state or defects. The emission peaks at 642 and 653 nm are observed to be broad and occurred at a lower energy value than that corresponding to the excitonic emission band, which can be attributed to surface defects that act as radiative or nonradiative centers or sulfur vacancies.[27] The PL results also suggest growth of nanoparticles governed by the "Ostwald ripening" mechanism. The smaller particles are thermodynamically less able because of their higher surface free energy.[28] Thus, as temperature was elevated; there was a slow diffusion of materials from small particles to the surface of larger particles. In Figure 2(c), the surfaces of HgS nanoparticles are coarse and consist of small grains, which also can prove "Ostwald ripening" mechanism. As a result, the particle size increases continuously during growth. Since the particle size is directly related to size-quantum effect of nanocrystals, which results in red-shift of UV-vis and PL spectra at higher temperature.

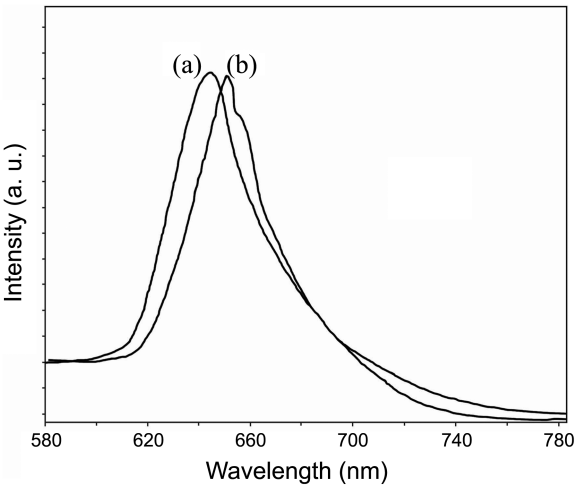

Figure 5. Photoluminescence (PL) spectra of HgS nanocrystals synthesized at (a) 60 ºC, (b) 75 ºC.

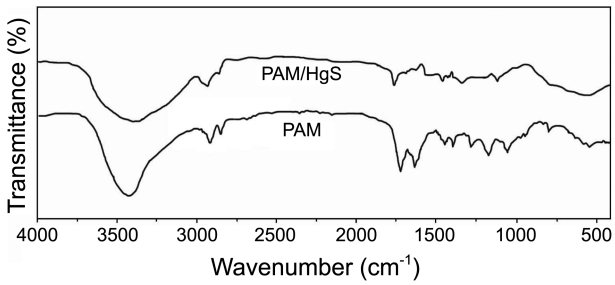

Figure 6. FT-IR spectra of PAM and PAM/HgS nanocomposites.

To investigate whether the surface of HgS nanocrystals was capped with PAM polymer, Fourier transform infrared (FT-IR) spectra of PAM and PAM/HgS nanocomposite were performed as shown in Figure 6. The IR peaks of PAM at 3412, 1668 and 1607 cm^{-1} are assigned to the stretching vibration of -NH_2, amide I (mainly C=O stretching vibrations) and amide II (the coupling of bending vibrations of -NH and stretching vibrations of -CN) bands, respectively.[29,30] It can be clearly seen that -NH_2 peak of PAM/HgS broadens and shifts low wave number, which indicates that these groups of PAM could interact with Hg^{2+}. The intensity of the characteristic amide I and amide II of PAM/HgS nanocomposites weaken compared to that of PAM, and the peak of amide II almost disappears, suggesting that the nitrogen and oxygen atom of the amide bond possibly interact with surface Hg. Consequently, the multiple interaction of PAM to Hg ions provided better stability of HgS nanocrystals. In FT-IR spectrum of PAM/HgS nanocomposites, there is not obvious IR peaks of HgS, which suggest that the products have good transmittance in infrared area. Due to infrared transmittance and good UV-vis adsorption of PAM/HgS nanocomposites, it could be used in application of infrared window materials, semiconductor devices and sensors. In addition, the results of FT-IR show that the obtained products are inorganic-polymer materials.

Thermogravimetric analysis (TGA) thermograms of PAM and PAM/HgS nanocomposites are shown in Figure 7. For the TGA curves of PAM and PAM/HgS, there are three stages of weight loss. The first stage of the decomposition observed from 50 to 150 ºC is due to the loss of absorbed water in both of PAM and PAM/HgS nanocomposites. From 150 to 300 ºC, the loss of weight is mainly owing to the escape of several kinds of small molecules. The third stage of the decomposition is observed from 300 to 550 ºC

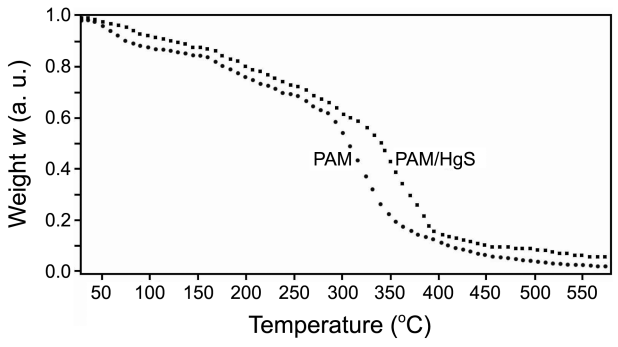

Figure 7. TGA curves for PAM and PAM/HgS nanocomposites.

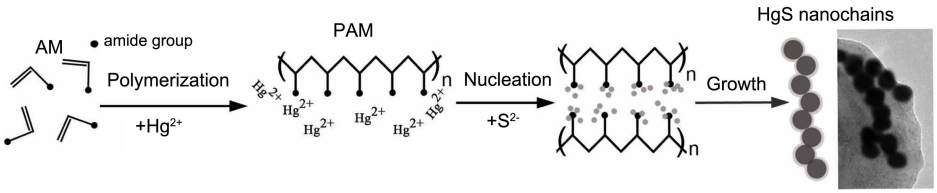

Figure 8. Illustration of the formation of PAM/HgS nanocomposites.

corresponding to the pyrolysis of PAM and volatilization of HgS. It can be seen that the thermal degradation of the PAM/HgS nanocomposites is different from that of the pure PAM. Introduction of HgS nanocrystals in PAM matrix shifts the onset of the thermal decomposition toward higher temperature. The enhancement of the thermal stability of PAM might be due to the chemical interaction between PAM and HgS nanocrystal rather than physical adsorption.

According to discussion above, the scheme of the formation of PAM/HgS nanocomposites is illustrated in Figure 8. At the first step of the preparation, by mixing monomer acrylamide, Hg^{2+} and AIBN complexes, there is a polymerization reaction which results in PAM polymer chains. As a soft Lewis acid, Hg^{2+} has a high affinity for -NH functional group of PAM. In addition, the negative charged oxygen atoms contained in carbonyl group (C=O) also interacts with Hg^{2+}. Therefore, PAM can provide multiple binding sites for Hg^{2+}, and the concentration of Hg^{2+} around the PAM chains is very high because of this interaction. When the S^{2-} is introduced to Hg^{2+}-PAM solution, it rapidly combines with Hg^{2+} to form HgS nuclei in binding sites of PAM because of small solubility product of HgS. In this step, the PAM plays very important role in reducing activation energy of nucleation as capping agent. Surface passivation helps to achieve size selectivity, prevent agglomeration and fusing of particles. The long carbon chain of PAM can provide great steric hindrance to control the size of HgS nanoparticle and result in chain-like HgS nanoparticles.

Conclusion

To summarize, HgS nanocrystals capped with PAM have been prepared using polymerization reaction method. The above synthesis process can be applied for other polymer-chalcogenide nanocomposites. The as-prepared products were characterized by means of several techniques including XRD, EDX, TEM, UV-vis, PL, FT-IR and TGA. The reaction temperature is a key factor to influence the size and morphology of HgS nanocrystals. The PAM plays an important role in the formation of HgS nanocrystals, Hg^{2+} and HgS can interact with functional groups of PAM. The possible mechanism was also investigated on the basis of experimental results. The obtained PAM/HgS nanocomposites showed good optical properties and infrared transmittance.

Acknowledgments. This study was supported by the Nature Science Foundation of the Education Department of Henan Province (13B150182) and the Key Nature Science Foundation of Pingdingshan University.

References

1. Qian, X.; Yin, J.; Feng, S.; Liu, S.; Zhu, Z. *J. Mater. Chem.* **2001**, *11*, 2504.
2. Su, C.; Liu, J.; Shao, C.; Liu, Y. *J. Non-Crystalline Solids* **2011**, *357*, 1488.
3. Chung, Y.; Yun, S.; Lee, C.; Jo, N.; Yo, C.; Ryu, K. *Bull. Korean Chem. Soc.* **2010**, *31*, 2065.
4. Kumar, V. V.; Nithya, S.; Shyam, A.; Subramanian, N. S.; Anthuvan, J. T.; Anthony, S. P. *Bull. Korean Chem. Soc.* **2013**, *34*, 2702.
5. Anthony, S. P. *Mater. Lett.* **2009**, *63*, 773.
6. Asai, T.; Sakamoto, W.; Yogo, T. *Mater. Lett.* **2013**, *107*, 235.
7. Morsali, A.; Panjehpour, A. *Inorganica Chimica Acta* **2012**, *391*, 210.
8. Guo, Y.; Zhang, J.; Yang, L.; Wang, H.; Wang, F.; Zheng, Z. *Chem. Comm.* **2010**, *46*, 3493.
9. Konopny, L.; Berfeld, M.; Popovitz-Biro, R.; Weissbuch, I.; Leiserowitz, L.; Lahav, M. *Adv. Mater.* **2001**, *13*, 580.
10. Abdollahian, Y.; Hauser, J. L.; Rogow, D. L.; Oliver, A. G.; Oliver, S. R. J. *Dalton Transactions* **2012**, *41*, 12630.
11. Ren, T.; Xu, S.; Zhao, W.; Zhu, J. *J. Photochem. Photobio. A: Chem.* **2005**, *173*, 93.
12. Soltani, N.; Saion, E.; Hussein, M. Z.; Erfani, M.; Rezaee, K.; Bahmanrokh, G. *J. Inorg. Organomet. Polym.* **2012**, *22*, 830.
13. Chen, C.; Wu, S.; Wang, Y.; Hou, J.; Ma, L.; Sun, X. *China J. Chinese Materia Medica* **2012**, *37*, 2968.
14. Zhang, L.; Yang, G.; He, G.; Wang, L.; Liu, Q.; Zhang, Q.; Qin, D. *Appl. Surf. Sci.* **2012**, *258*, 8185.
15. Qin, D. Z.; Ma, X. M.; Yang, L.; Zhang, L.; Ma, Z. J.; Zhang, J. *J. Nanopart. Res.* **2008**, *10*, 559.
16. Wichiansee, W.; Nordin, M. N.; Green, M.; Curry, R. J. *J. Mater. Chem.* **2011**, *21*, 7331.
17. Liu, X.; Liu, R.; Tang, Y.; Zhang, L.; Hou, X.; Lv, Y. *Analyst*, **2012**, *137*, 1473.
18. Sobhani, A.; Salavati-Niasari, M.; Sobhani, M. *Mater. Sci. Semicon. Proc.* **2013**, *16*, 410.
19. Marimuthu, G.; Ramalingam, K.; Rizzoli, C.; Arivanandhan, M. *J. Nanopart. Res.* **2012**, *14*, 710.
20. Qian, X.; Yin, J.; Huang, J.; Yang, Y.; Guo, X.; Zhu, Z. *Mater. Chem. Phys.* **2001**, *68*, 95.
21. Sundarrajan, P.; Eswaran, P.; Marimuthu, A.; Subhadra, L. B.; Kannaiyan, P. *Bull. Korean Chem. Soc.* **2012**, *33*, 3218.
22. Basyach, P.; Choudhury, A. *Mater. Res. Bull.* **2013**, *48*, 2543.
23. Li, D.; Xie, H.; Liu, J.; Duan, C. *J. Exp. Nanosci.* **2011**, *6*, 209.
24. Wang, X.; Zhang, S.; Zhang, Z. *Mater. Chem. Phys.* **2008**, *107*, 9.
25. Salavati-Niasari, M.; Bazarganipour, M.; Davar, F. *J. Alloys Compounds* **2010**, *499*, 121.
26. Wilson, W. L.; Szajowski, P. F.; Brus, L. E. *Science* **1993**, *262*, 1242.
27. Mahdi, M. A.; Ramizy, A.; Hassan, Z.; Ng, S. S.; Hassan, J. J.; Kasim, S. J. *Chalcogendie Lett.* **2012**, *9*, 19.
28. Priyam, A.; Chatterjee, A.; Das, S. K.; Saha, A. *Res. Chem. Intermed.* **2005**, *31*, 691.
29. Mishra, S.; Sen, G.; Rani, G. U.; Sinha, S. *International J. Biological Macromolecules* **2011**, *49*, 591.
30. Patra, S. K.; Swain, S. K. *J. Applied Polymer Sci.* **2011**, *120*, 1533.